

Frozen Gaussian Approximation for the Dirac Equation in Curved Space with Application to Strained Graphene

Lihui Chai¹, Lorin Emmanuel^{2,*} and Xu Yang³

¹ School of Mathematics, Sun Yat-sen University, Guangzhou, China.

² School of Mathematics and Statistics, Carleton University, Ottawa, Canada. Centre de Recherches Mathématiques, Université de Montréal, Montréal, Canada.

³ Department of Mathematics, University of California, Santa Barbara, USA.

Received 25 October 2021; Accepted (in revised version) 15 November 2022

Abstract. In this paper, we derive the frozen Gaussian approximation (FGA) for computing the solution to the Dirac equation in curved space in the semi-classical regime. The latter equation is used in particular for modeling electronic scattering on strained graphene surfaces. We present numerical comparisons of the Dirac solutions on curved and flat spaces, illustrating the focusing effect of graphene surfaces, as well as qualitative comparisons with a tight-binding model. A CPU-time comparison shows that FGA becomes more efficient than an IMEX pseudospectral method when the semiclassical parameter is small.

AMS subject classifications: 35Q41, 81Q05, 81Q20, 78A05

Key words: Dirac equation, semi-classical regime, frozen Gaussian approximation, strained graphene.

1 Introduction

In this paper, we are interested in computing the solution of a massless two-dimensional Dirac equation in curved space in the low energy limit (semi-classical regime), modeling electron motions on strained graphene surfaces [5, 9, 22, 25, 26]. Some connections with refractive optics can also be obtained through Evans' model [13]. Mathematically, the Dirac equation in curved space is a non-conservative first-order hyperbolic system.

*Corresponding author. *Email addresses:* chailihui@mail.sysu.edu.cn (L. Chai), elorin@math.carleton.ca (E. Lorin), xuyang@math.ucsb.edu (X. Yang)

Although the Dirac equation under consideration is linear, it has non-constant (space-dependent) coefficients and possesses, compared to the Dirac equation in flat space, additional order-zero terms (corresponding physically to spin connections); see [14]. The latter is, however, perturbative in the semi-classical regime.

The Frozen Gaussian Approximation (FGA) is one of the most accurate and efficient methods for computing the solution to wave equations, including the Dirac equation, in the semi-classical regime. FGA was first developed by Herman-Kluk (HK) [16] for computing the solution to the Schrödinger equation in the semi-classical regime, and it was mathematically analyzed in [27]. More recently, the HK-formalism was used and analyzed to derive fast numerical solvers in the semi-classical regime for different classes of partial differential equations: the Schrödinger equation [32], the classical wave equation [19,20] and general linear hyperbolic systems of conservation laws [21]. The analysis of FGA for the Dirac equation in flat space was given in [7], and an alternative efficient Gaussian beam method was proposed in [31] for solving the Dirac equation in flat space in the semi-classical regime.

The objective of this work is to describe the trajectories of electrons on a given strained graphene surface. To achieve this goal, we will proceed as follows:

- Establish the two-dimensional (2D) massless Dirac equation in curved space (\mathcal{S}) and in semi-classical regime.
- Solve this Dirac equation in curved space by FGA.
- Compute the classical or semi-classical electron trajectories thanks to the Hamiltonian flow used in FGA. In particular, we shall present focusing effects of strained graphene.

Let us first discuss the interest in using FGA for the Dirac equation modeling strained graphene surfaces. The most advanced models, beyond *ab initio* calculations (which are not realistic for a large number of atoms), are based on density functional theory (and Kohn-Sham equations). These models are very computationally complex, so that for graphene, tight-binding models are usually preferred as they allow for far more efficient computations, while still keeping a good modeling accuracy. Moreover, it is well-known that interesting properties of 2D materials often occur at low energy; from the effective Hamiltonian obtained by Bloch transform on the tight-binding operator [6, 17], the expansion of the dispersion relation about the so-called Dirac points (zeros of effective Hamiltonian eigenvalues) allows to obtain a continuum theory-based massless 2D Dirac equation, and with non-constant coefficients in the case of strained graphene). In graphene, the distance between Carbon atoms is typically much smaller than the scale of the deformation, so that the semi-classical regime (denoting ε as the small parameter) is usually considered [24]. However, the direct numerical computation of the Dirac equation in the semi-classical regime requires mesh size typically in $\mathcal{O}(\varepsilon)$ or even smaller, therefore the computational time is inversely proportional to ε on a fine grid, leading to expensive or unaffordable computational cost. In addition, non-constant coefficients

of the Dirac Hamiltonian make the accurate and stable approximation of this equation even more complex. Hence, FGA is an alternative choice that allows for an accurate and efficient way of solving the Dirac equation in the semi-classical regime and with better modeling accuracy than a classical model. Let us add that the FGA algorithm is embarrassingly parallel [8].

Hereafter, we shall derive the FGA formulation for the Dirac equation modeling the transport of electrons on strained graphene surfaces. For clarity, we shortly recall the derivation of the Dirac equation itself.

1.1 Derivation of the Dirac equation

Consider a bounded 2D surface \mathcal{S} embedded in \mathbb{R}^3 , and parameterized in Cartesian coordinates as follows

$$\mathcal{S} = \{(\mathbf{x}, Z(\mathbf{x})) / \mathbf{x} \in \mathcal{D}\}, \quad (1.1)$$

with $Z \in C^1(\mathcal{D}; \mathbb{R})$ and $\mathbf{x} = (x, y) \in \mathcal{D} \subset \mathbb{R}^2$. We denote $\mathbf{r}(\mathbf{x}) = (\mathbf{x}, Z(\mathbf{x})) \in \mathbb{R}^3$. In this set of coordinates, the Dirac equation modeling strained graphene surfaces is extremely complex [14]. As a consequence, in order to simplify the Dirac equation expression, it was proposed in [14] to use the commonly called isothermal coordinates [1, 10, 29]. This choice of coordinates is motivated by the fact that they allow for a simple expression of the corresponding Dirac Hamiltonian "independently" of the complexity of the smooth graphene surface. Alternative systems of coordinates, such as cylindrical or spherical coordinates are naturally used but for very specific graphene structures. Let us notice that Dirac Hamiltonians for strained graphene are derived directly from a Tight-Binding model in the low energy limit, where the lattice of Carbon atoms is assumed to be subject to external mechanical forces modeled by strain/stress tensors or directly from a displacement field. We refer to [24] for details.

We recall that isothermal coordinates $\mathbf{u} = (u, v)$ are local orthogonal coordinates on \mathcal{S} , for which the metric is given by

$$ds^2 = \rho(\mathbf{u}) [du^2 + dv^2]. \quad (1.2)$$

In these coordinates, the corresponding metric tensor is diagonal:

$$g(\mathbf{u}) = \begin{bmatrix} 1 & 0 & 0 \\ 0 & -\rho(\mathbf{u}) & 0 \\ 0 & 0 & -\rho(\mathbf{u}) \end{bmatrix}, \quad (1.3)$$

and the natural vielbein is defined as:

$$e(\mathbf{u}) = \begin{bmatrix} 1 & 0 & 0 \\ 0 & \sqrt{\rho(\mathbf{u})} & 0 \\ 0 & 0 & \sqrt{\rho(\mathbf{u})} \end{bmatrix}. \quad (1.4)$$

The relation between the Cartesian and isothermal coordinates is obtained thanks to the Beltrami equation.

Definition 1.1. Let the coordinates be expressed in the complex plane as $z = x + iy \in \mathbb{C}$ and $w = u + iv \in \mathbb{C}$. A mapping from the Cartesian to isothermal coordinates $z \rightarrow w$ is said quasi-conformal if it is a solution to the Beltrami equation:

$$w_{\bar{z}} = \mu(z)w_z, \tag{1.5}$$

where μ is such that $\|\mu\|_\infty < 1$, and is called the Beltrami coefficient.

In isothermal coordinates, $ds^2 = \rho dw d\bar{w}$ with

$$\rho(z) = \frac{\lambda(z)}{|w_z(z)|^2}, \quad \lambda = \frac{1}{4}(E + G + 2\sqrt{\Delta}), \quad \mu = \frac{E - G + 2iF}{4\lambda}, \tag{1.6}$$

and $\Delta = \det(g_S)$ and $E = 1 + Z_x^2$, $G = 1 + Z_y^2$ and $F = Z_x Z_y$. Practically, the construction of the isothermal coordinates is obtained thanks to the solution to the Beltrami equation which can be rewritten in the following form

$$\nabla u(\mathbf{x}) = JA \nabla v(\mathbf{x}), \tag{1.7}$$

where A and J are defined as

$$A := \frac{1}{1 - |\mu|^2} \times \begin{bmatrix} (\operatorname{Re}(\mu) - 1)^2 + \operatorname{Im}(\mu)^2 & -2\operatorname{Im}(\mu) \\ -2\operatorname{Im}(\mu) & (1 + \operatorname{Re}(\mu))^2 + \operatorname{Im}(\mu)^2 \end{bmatrix}, \quad J := \begin{bmatrix} 0 & -1 \\ 1 & 0 \end{bmatrix},$$

and we give more detailed derivation in [14].

1.2 Dirac equation in curved space

Here we assume that ρ is a given surface-dependent smooth function, previously computed. We are interested in the evolution of electrons on this surface. The corresponding massless Dirac equation (two-equation system) we hence consider, reads

$$i\hbar \partial_t \psi(t, \mathbf{u}) = \left\{ -i\hbar \frac{v_F}{\sqrt{\rho(\mathbf{u})}} \sigma^i \left[\partial_i - i \frac{1}{\hbar} A_i(\mathbf{u}) + \Omega_i(\mathbf{u}) \right] \right\} \psi(t, \mathbf{u}), \tag{1.8}$$

where A_i is a pseudo-magnetic field, the affine spin connection is $\Omega_i = i\omega_i(\mathbf{u})\sigma^0$, and

$$\omega_1(\mathbf{u}) = \frac{1}{4} \frac{\rho_v(\mathbf{u})}{\rho(\mathbf{u})} = \frac{1}{4} \partial_v \ln \rho(\mathbf{u}), \quad \omega_2(\mathbf{u}) = -\frac{1}{4} \frac{\rho_u(\mathbf{u})}{\rho(\mathbf{u})} = -\frac{1}{4} \partial_u \ln \rho(\mathbf{u}). \tag{1.9}$$

We will also denote $\boldsymbol{\omega} = (\omega_1, \omega_2)^T$. We recall that the Pauli matrices are defined as follows [28]:

$$\sigma^0 = \begin{bmatrix} 1 & 0 \\ 0 & -1 \end{bmatrix}, \quad \sigma^1 = \begin{bmatrix} 0 & 1 \\ 1 & 0 \end{bmatrix}, \quad \sigma^2 = \begin{bmatrix} 0 & -i \\ i & 0 \end{bmatrix}. \quad (1.10)$$

It is well-known that in curved space, because of the affine spin connection, the Dirac Hamiltonian is not Hermitian. In order to hermiticize the Hamiltonian, we proceed as follows: $H_\eta = \eta H \eta^{-1}$ such that $H_\eta^\dagger = H_\eta$. It is proposed in [14] to take $\eta = \sqrt[4]{\det(g(\mathbf{u}))}$, where g is the metric tensor on the surface \mathcal{S} . In the case of isothermal coordinates $\det(g)(\mathbf{u}) = \rho^2(\mathbf{u})$. Hence

$$H_\eta = \sqrt{\rho(\mathbf{u})} H \sqrt{\rho(\mathbf{u})}^{-1} = -i\hbar \frac{v_F}{\sqrt{\rho(\mathbf{u})}} \sigma^i \left[\partial_i - i \frac{1}{\hbar} A_i(\mathbf{u}) + C_i(\mathbf{u}) \right], \quad (1.11)$$

where we now have defined

$$C_1(\mathbf{u}) = -\frac{\rho_u(\mathbf{u})}{4\rho(\mathbf{u})} = \omega_2(\mathbf{u}), \quad C_2(\mathbf{u}) = -\frac{\rho_v(\mathbf{u})}{4\rho(\mathbf{u})} = -\omega_1(\mathbf{u}). \quad (1.12)$$

We are hence interested in the solution of the massless Dirac equation in curved space and semi-classical regime and described by the Hamiltonian (1.11). For the sake of notation simplicity, hereafter we will denote by x the isothermal coordinates.

1.3 Semi-classical electron trajectories

Thanks to the solution to the Hamiltonian flow, frozen Gaussian approximation (FGA) allows for a computation of classical trajectories of electrons by

$$\begin{cases} \frac{d\mathbf{Q}}{dt} = \partial_P h(\mathbf{Q}, \mathbf{P}), & \mathbf{Q}(0, \mathbf{q}, \mathbf{p}) = \mathbf{q}, \\ \frac{d\mathbf{P}}{dt} = -\partial_Q h(\mathbf{Q}, \mathbf{P}), & \mathbf{P}(0, \mathbf{q}, \mathbf{p}) = \mathbf{p}, \end{cases}$$

with $h(\mathbf{Q}, \mathbf{P}) = s(\mathbf{Q}) |\mathbf{P} - \mathbf{A}(\mathbf{Q})|$, and $s(\mathbf{Q}) = v_F / \sqrt{\rho(\mathbf{Q})}$ where v_F the Fermi velocity for unstrained graphene. Moreover \mathbf{Q} (resp. \mathbf{P}) denotes the Gaussian profiles (resp. momentum function). Typically \mathbf{Q} describes the trajectories of a classical particle, initially located in \mathbf{q} . Although the full computation of the FGA allows in particular for the computation the electron trajectories on a given surface, the latter can be rewritten as the Newton-like equation:

$$\frac{d^2 \mathbf{Q}}{dt^2} = -\partial_{PP} h(\mathbf{Q}, \mathbf{P}) \partial_Q h(\mathbf{Q}, \mathbf{P}) + \partial_{QP} h(\mathbf{Q}, \mathbf{P}) \partial_P h(\mathbf{Q}, \mathbf{P}), \quad \mathbf{Q}(0, \mathbf{q}, \mathbf{p}) = \mathbf{q}, \quad \mathbf{P}(0, \mathbf{q}, \mathbf{p}) = \mathbf{p}.$$

If we neglect A , the classical trajectories are modeled by Evans' model [13] and which only requires the solution to a simple second order ODE system :

$$\begin{cases} \frac{d^2 Q}{dt^2} = \frac{1}{2} \nabla \rho(Q), \\ \left| \frac{dQ(0)}{dt} \right| = n_0, \\ Q(0) = Q_0, \end{cases} \quad (1.13)$$

where n_0 is the common refractive index at the "origin" of the rays, and where the "initial position" Q_0 . More related discussions can be found in [4, 11]. The electron trajectories can then modeled by (1.13) or more accurately by the Dirac equation in curved space and semi-classical regime, which is the purpose of this paper.

1.4 Organization

The rest of the paper is organized as follows. In Section 2, we derive the FGA for the Dirac equation in curved space. Section 3 is devoted to some numerical experiments. We recall the basics of the computational aspects of the FGA. We then numerically compare the propagation of a wave-packet on flat and curved surfaces in order to illustrate the focusing effect of strained graphene in this regime. We also present some simulations of the semi-classical propagation of electrons along the surface, and some comparisons with tight-binding and Evans' models. We conclude in Section 4.

2 Frozen Gaussian approximation for the Dirac equation

To consider the Dirac equation in the semi-classical regime, we first rewrite the equation such that there remains only one dimensionless parameter $\varepsilon = \hbar/L$, which is obtained by replacing $\mathbf{u} \rightarrow \mathbf{x}/L$, $t \rightarrow t/T$, and $\boldsymbol{\psi}(t, \mathbf{u}) \rightarrow L^{-1} \boldsymbol{\psi}^\varepsilon(t/T, \mathbf{u}/L)$, with $L = Tv_F$. The dimensionless Dirac equation is then obtained in the form of

$$i\varepsilon \partial_t \boldsymbol{\psi}^\varepsilon(t, \mathbf{x}) = -s(\mathbf{x}) (i\varepsilon \hat{\sigma} \cdot \nabla + \hat{\sigma} \cdot \mathbf{A}(\mathbf{x}) + i\varepsilon \hat{\sigma} \cdot \mathbf{C}(\mathbf{x})) \boldsymbol{\psi}^\varepsilon(t, \mathbf{x}), \quad (2.1)$$

$$\boldsymbol{\psi}^\varepsilon(0, \mathbf{x}) = \boldsymbol{\varphi}_I^\varepsilon(\mathbf{x}) = \omega_I(\mathbf{x}) \exp\left(\frac{i}{\varepsilon} S_I(\mathbf{x})\right). \quad (2.2)$$

Here $s(\mathbf{x}) = 1/\sqrt{\rho(\mathbf{x})}$, $\boldsymbol{\psi}^\varepsilon = (\psi_1^\varepsilon, \psi_2^\varepsilon)^T \in \mathbb{C}^2$ is the spinor, $\mathbf{C} = (C_1, C_2)$ defined in (1.12), and S_I (resp. ω_I) is the initial phase (resp. amplitude). We explicitly have

$$-is(\mathbf{x}) \hat{\sigma} \cdot \mathbf{C}(\mathbf{x}) = s(\mathbf{x}) \begin{bmatrix} 0 & -C_2(\mathbf{x}) - iC_1(\mathbf{x}) \\ C_2(\mathbf{x}) - iC_1(\mathbf{x}) & 0 \end{bmatrix}. \quad (2.3)$$

2.1 Characteristic fields

The symbol of the Dirac operator which is studied in this paper reads as follows

$$D_\varepsilon(\mathbf{q}, \mathbf{p}) := s(\mathbf{q}) \hat{\sigma} \cdot (\mathbf{p} - \mathbf{A}(\mathbf{q}) - i\varepsilon \mathbf{C}), \quad (2.4)$$

and we denote by

$$D(\mathbf{q}, \mathbf{p}) := s(\mathbf{q}) \hat{\sigma} \cdot (\mathbf{p} - \mathbf{A}(\mathbf{q})), \quad (2.5)$$

the $\mathcal{O}(1)$ contribution in D_ε . Set $\mathbf{w}(\mathbf{q}, \mathbf{p}) = s(\mathbf{q})(\mathbf{p} - \mathbf{A}(\mathbf{q})) = (s(\mathbf{q})(p_1 - A_1(\mathbf{q})), s(\mathbf{q})(p_2 - A_2(\mathbf{q})))^T$ and

$$D(\mathbf{q}, \mathbf{p}) = \begin{bmatrix} 0 & w_1(\mathbf{q}, \mathbf{p}) - iw_2(\mathbf{q}, \mathbf{p}) \\ w_1(\mathbf{q}, \mathbf{p}) + iw_2(\mathbf{q}, \mathbf{p}) & 0 \end{bmatrix}. \quad (2.6)$$

The corresponding eigenvalues are given by

$$h_\pm(\mathbf{q}, \mathbf{p}) = \pm \lambda(\mathbf{q}, \mathbf{p}), \quad \text{where } \lambda(\mathbf{q}, \mathbf{p}) = |\mathbf{w}(\mathbf{q}, \mathbf{p})| = s(\mathbf{q}) |\mathbf{p} - \mathbf{A}(\mathbf{q})|.$$

Denote the corresponding eigenvectors as \mathbf{r}_m , $m = \pm$,

$$\begin{aligned} \mathbf{r}_+ &= \frac{1}{r} \begin{pmatrix} |\mathbf{w}| \\ \omega_1 + i\omega_2 \end{pmatrix}, \\ \mathbf{r}_- &= \frac{1}{r} \begin{pmatrix} -|\mathbf{w}| \\ \omega_1 + i\omega_2 \end{pmatrix}, \end{aligned} \quad (2.7)$$

where $r = \sqrt{2}|\mathbf{w}|$ and $|\mathbf{w}(\mathbf{q}, \mathbf{p})| = s(\mathbf{q}) \sqrt{|\mathbf{p}|^2 + |\boldsymbol{\omega}(\mathbf{q})|^2}$ and

$$\partial_{\mathbf{w}} \mathbf{r}_\pm = \frac{1}{\sqrt{2}|\mathbf{w}|} \frac{1}{|\mathbf{w}|^2} \begin{pmatrix} 0 & w_2^2 - iw_1w_2 \\ 0 & iw_1^2 - w_1w_2 \end{pmatrix}. \quad (2.8)$$

We leave the detailed computation of the eigenvalues and eigenvectors to the Appendix.

2.2 Derivation of the FGA

This subsection is dedicated to the complete derivation of FGA for the Dirac equation in curved space. Starting from the standard ansatz

$$\begin{aligned} \psi^\varepsilon &= \frac{1}{(2\pi\varepsilon)^3} \sum_{m=\pm} \int_{\mathbb{R}^6} (a_m(t, \mathbf{q}, \mathbf{p}) + \varepsilon \beta_m(t, \mathbf{q}, \mathbf{p})) \\ &\quad \times \exp\left(\frac{i}{\varepsilon} \Phi_m(t, \mathbf{y}, \mathbf{q}, \mathbf{p})\right) v_m(\mathbf{y}, \mathbf{q}, \mathbf{p}) \, d\mathbf{y} d\mathbf{q} d\mathbf{p}, \end{aligned} \quad (2.9)$$

where

$$\begin{aligned} \Phi_m(t, \mathbf{y}, \mathbf{q}, \mathbf{p}) = & S(t, \mathbf{q}, \mathbf{p}) + \frac{i}{2} |\mathbf{x} - \mathbf{Q}_m(t, \mathbf{q}, \mathbf{p})|^2 + \mathbf{P}_m \cdot (\mathbf{x} - \mathbf{Q}_m(t, \mathbf{q}, \mathbf{p})) \\ & + \frac{i}{2} |\mathbf{y} - \mathbf{q}|^2 - \mathbf{p} \cdot (\mathbf{y} - \mathbf{q}), \end{aligned} \tag{2.10}$$

$$\mathbf{a}_m(t, \mathbf{q}, \mathbf{p}) = a_m(t, \mathbf{q}, \mathbf{p}) \mathbf{r}_m(\mathbf{Q}_m, \mathbf{P}_m), \tag{2.11}$$

$$\mathbf{v}_m(\mathbf{y}, \mathbf{q}, \mathbf{p}) = \mathbf{r}_m(\mathbf{q}, \mathbf{p}) \cdot \boldsymbol{\psi}_1^\varepsilon(\mathbf{y}). \tag{2.12}$$

In order to perform the asymptotics, we introduce the following definition

Definition 2.1. Two functions f and g are said equivalent if

$$f \sim g \Leftrightarrow \int f e^{i\Phi/\varepsilon} d\mathbf{y} d\mathbf{q} d\mathbf{p} = \int g e^{i\Phi/\varepsilon} d\mathbf{y} d\mathbf{q} d\mathbf{p}.$$

Let's denote

$$\partial_z = \partial_q - i\partial_p, \quad Z = \partial_z(\mathbf{Q} + i\mathbf{P}).$$

Then based on Definition 2.1 and following the techniques in [20], one can easily show that

Lemma 2.1. For any vector $\mathbf{b}(\mathbf{y}, \mathbf{q}, \mathbf{p}) = (b_j)$ and matrix $G(\mathbf{y}, \mathbf{q}, \mathbf{p}) = (G_{jk})$ in Schwartz class component-wisely, one has the flowing integration by parts formula

$$\begin{aligned} b_j(\mathbf{x} - \mathbf{Q})_j & \sim -\varepsilon \partial_{z_k} (b_j Z_{jk}^{-1}), \\ (\mathbf{x} - \mathbf{Q})_j G_{jk} (\mathbf{x} - \mathbf{Q})_k & \sim \varepsilon \partial_{z_k} Q_l G_{lj} Z_{jk}^{-1} + \varepsilon^2 \partial_{z_m} \left(\partial_{z_n} (G_{jk} Z_{kn}^{-1}) Z_{jm}^{-1} \right), \end{aligned}$$

where Einstein's summation convention has been used. Moreover, $(\mathbf{x} - \mathbf{Q})^a \sim \mathcal{O}(\varepsilon^{|a|/2})$ for $|a| > 2$.

We now derive explicitly the three fundamental equations allowing for the construction of the FGA.

1. *Gaussian profile \mathbf{Q} and momentum function \mathbf{P} .* As for any FGA, the bi-center \mathbf{Q} and \mathbf{P} simply satisfy the Hamiltonian flow:

$$\begin{cases} \frac{d\mathbf{Q}}{dt} = \partial_P h(\mathbf{Q}, \mathbf{P}), & \mathbf{Q}(0, \mathbf{q}, \mathbf{p}) = \mathbf{q}, \\ \frac{d\mathbf{P}}{dt} = -\partial_Q h(\mathbf{Q}, \mathbf{P}), & \mathbf{P}(0, \mathbf{q}, \mathbf{p}) = \mathbf{p}. \end{cases} \tag{2.13}$$

We then determine the evolution equation for the action function.

Notice that $h(\mathbf{Q}, \mathbf{P}) = s(\mathbf{Q}) |\mathbf{P} - \mathbf{A}(\mathbf{Q})|$ is not differentiable at singular points $\mathbf{P} = \mathbf{A}(\mathbf{Q})$, where the above equation system is not well-defined. However, if we assume initially $\mathbf{p} \neq \mathbf{A}(\mathbf{q})$, then we can guarantee that the singularity would not be touched by the Hamiltonian dynamics.

2. *Action function S.* In order to derive the evolution equation for the action function S , preliminary computations are needed. By definition of Φ , we have

$$\partial_t \Phi = \partial_t S - \mathbf{P} \cdot \partial_t \mathbf{Q} + (\mathbf{x} - \mathbf{Q}) \cdot \partial_t (\mathbf{P} - i\mathbf{Q}), \quad (2.14)$$

$$\nabla_x \Phi = i(\mathbf{x} - \mathbf{Q}) + \mathbf{P}. \quad (2.15)$$

Then taking derivatives to (2.9) gives

$$\begin{aligned} \partial_t \psi^\varepsilon &= \int \left(\partial_t \mathbf{a} + \varepsilon \partial_t \boldsymbol{\beta} + \frac{i}{\varepsilon} \partial_t \Phi (\mathbf{a} + \varepsilon \boldsymbol{\beta}) \right) e^{i\Phi/\varepsilon} v d\mathbf{y} d\mathbf{q} d\mathbf{p} \\ &= \int \left(\partial_t \mathbf{a} + \frac{i}{\varepsilon} (\partial_t S - \mathbf{P} \cdot \partial_t \mathbf{Q} + (\mathbf{x} - \mathbf{Q}) \cdot \partial_t (\mathbf{P} - i\mathbf{Q})) \mathbf{a} \right) e^{i\Phi/\varepsilon} v d\mathbf{y} d\mathbf{q} d\mathbf{p} \\ &\quad + \int (\varepsilon \partial_t \boldsymbol{\beta} + i(\partial_t S - \mathbf{P} \cdot \partial_t \mathbf{Q} + (\mathbf{x} - \mathbf{Q}) \cdot \partial_t (\mathbf{P} - i\mathbf{Q})) \boldsymbol{\beta}) e^{i\Phi/\varepsilon} v d\mathbf{y} d\mathbf{q} d\mathbf{p}, \end{aligned} \quad (2.16)$$

$$\nabla_x \psi^\varepsilon = \int \frac{i}{\varepsilon} (i(\mathbf{x} - \mathbf{Q}) + \mathbf{P}) (\mathbf{a} + \varepsilon \boldsymbol{\beta}) e^{i\Phi/\varepsilon} v d\mathbf{y} d\mathbf{q} d\mathbf{p}. \quad (2.17)$$

Let's denote $B = -\hat{\sigma} \cdot \mathbf{A}$. We now expand B about \mathbf{Q}

$$B(\mathbf{x}) = B(\mathbf{Q}) + (\mathbf{x} - \mathbf{Q}) \cdot \partial_{\mathbf{Q}} B(\mathbf{Q}) + \frac{1}{2} (\mathbf{x} - \mathbf{Q})^2 : \partial_{\mathbf{Q}}^2 B(\mathbf{Q}) + \mathcal{O}(\mathbf{x} - \mathbf{Q})^3, \quad (2.18)$$

and expand s about \mathbf{Q}

$$s(\mathbf{x}) = s(\mathbf{Q}) + (\mathbf{x} - \mathbf{Q}) \cdot \partial_{\mathbf{Q}} s(\mathbf{Q}) + \frac{1}{2} (\mathbf{x} - \mathbf{Q})^2 : \partial_{\mathbf{Q}}^2 s(\mathbf{Q}) + \mathcal{O}(\mathbf{x} - \mathbf{Q})^3. \quad (2.19)$$

Substitute these into (2.1), to the order of $\mathcal{O}(\varepsilon^0)$, we get

$$- \int (\partial_t S - \mathbf{P} \cdot \partial_t \mathbf{Q}) \mathbf{a} e^{i\Phi/\varepsilon} v d\mathbf{y} d\mathbf{q} d\mathbf{p} = \int s(\mathbf{Q}) (\hat{\sigma} \cdot \mathbf{P} + B(\mathbf{Q})) \mathbf{a} e^{i\Phi/\varepsilon} v d\mathbf{y} d\mathbf{q} d\mathbf{p}. \quad (2.20)$$

As $\mathbf{a}(t, \mathbf{q}, \mathbf{p}) = a(t, \mathbf{q}, \mathbf{p}) \mathbf{r}(\mathbf{Q}, \mathbf{P})$, then the above equation holds if the action function S satisfies the following evolution equation

$$\partial_t S = \mathbf{P} \cdot \partial_t \mathbf{Q} - h(\mathbf{Q}, \mathbf{P}). \quad (2.21)$$

3. *Amplitude evolution equation.* We now construct the evolution equation for \mathbf{a} .

To the order of ε^1 ,

$$\begin{aligned} & \int i\varepsilon \left(\partial_t \mathbf{a} + \frac{i}{\varepsilon} (\mathbf{x} - \mathbf{Q}) \cdot \partial_t (\mathbf{P} - i\mathbf{Q}) \mathbf{a} + i(\partial_t S - \mathbf{P} \cdot \partial_t \mathbf{Q}) \boldsymbol{\beta} \right) e^{i\Phi/\varepsilon} v \, dy \, dq \, dp \\ &= \int \left\{ i s(\mathbf{Q}) \hat{\sigma} \cdot (\mathbf{x} - \mathbf{Q}) \mathbf{a} + s(\mathbf{Q}) (\mathbf{x} - \mathbf{Q}) \cdot \partial_{\mathbf{Q}} B \mathbf{a} \right. \\ & \quad + \frac{1}{2} s(\mathbf{Q}) (\mathbf{x} - \mathbf{Q})^2 : \partial_{\mathbf{Q}}^2 B \mathbf{a} + \varepsilon D \boldsymbol{\beta} - i\varepsilon s(\mathbf{Q}) \hat{\sigma} \cdot \mathbf{C}(\mathbf{Q}) \mathbf{a} \\ & \quad \left. + \left((\mathbf{x} - \mathbf{Q}) \cdot \partial_{\mathbf{Q}} s(\mathbf{Q}) + \frac{1}{2} (\mathbf{x} - \mathbf{Q})^2 : \partial_{\mathbf{Q}}^2 s(\mathbf{Q}) \right) (\hat{\sigma} \cdot \mathbf{P} + B(\mathbf{Q})) \mathbf{a} \right\} e^{i\Phi/\varepsilon} v \, dy \, dq \, dp, \end{aligned}$$

which implies,

$$\begin{aligned} & \int \left(\partial_t \mathbf{a} + \frac{1}{\varepsilon} (\mathbf{x} - \mathbf{Q}) \cdot \partial_t (\mathbf{Q} + i\mathbf{P}) \mathbf{a} + i(D(\mathbf{Q}, \mathbf{P}) - h(\mathbf{Q}, \mathbf{P})) \boldsymbol{\beta} \right) e^{i\Phi/\varepsilon} v \, dy \, dq \, dp \\ &= \int \left\{ \frac{1}{\varepsilon} s(\mathbf{Q}) \hat{\sigma} \cdot (\mathbf{x} - \mathbf{Q}) + \frac{1}{i\varepsilon} s(\mathbf{Q}) (\mathbf{x} - \mathbf{Q}) \cdot \partial_{\mathbf{Q}} B + \frac{1}{2i\varepsilon} s(\mathbf{Q}) (\mathbf{x} - \mathbf{Q})^2 : \partial_{\mathbf{Q}}^2 B - s(\mathbf{Q}) \hat{\sigma} \cdot \mathbf{C}(\mathbf{Q}) \right. \\ & \quad \left. + \frac{1}{i\varepsilon} \left((\mathbf{x} - \mathbf{Q}) \cdot \partial_{\mathbf{Q}} s(\mathbf{Q}) + \frac{1}{2} (\mathbf{x} - \mathbf{Q})^2 : \partial_{\mathbf{Q}}^2 s(\mathbf{Q}) \right) (\hat{\sigma} \cdot \mathbf{P} + B(\mathbf{Q})) \right\} a e^{i\Phi/\varepsilon} v \, dy \, dq \, dp. \end{aligned} \tag{2.22}$$

Applying the results in Lemma 2.1 gives

$$\begin{aligned} & \int \left(\partial_t \mathbf{a} v - \partial_{z_k} \left(\partial_t (\mathbf{Q}_j + i\mathbf{P}_j) Z_{jk}^{-1} \mathbf{a} v \right) + i(D(\mathbf{Q}, \mathbf{P}) - h(\mathbf{Q}, \mathbf{P})) \boldsymbol{\beta} v \right) e^{i\Phi/\varepsilon} \, dy \, dq \, dp \\ &= \int \left\{ -\partial_{z_k} \left(s \hat{\sigma}_j Z_{jk}^{-1} \mathbf{a} v \right) + i \partial_{z_k} \left(s \partial_j B Z_{jk}^{-1} \mathbf{a} v \right) - \frac{i}{2} s \partial_{z_k} Q_l \partial_{l_j} B Z_{jk}^{-1} \mathbf{a} v - s(\mathbf{Q}) \hat{\sigma} \cdot \mathbf{C}(\mathbf{Q}) \mathbf{a} v \right. \\ & \quad \left. + i \partial_{z_k} \left(\partial_j s Z_{jk}^{-1} (\hat{\sigma} \cdot \mathbf{P} + B) \mathbf{a} v \right) - \frac{i}{2} \partial_{z_k} Q_l \partial_{l_j} s Z_{jk}^{-1} (\hat{\sigma} \cdot \mathbf{P} + B) \mathbf{a} v \right\} e^{i\Phi/\varepsilon} \, dy \, dq \, dp, \end{aligned} \tag{2.23}$$

using Definition 2.1, we get

$$\begin{aligned} & i(h(\mathbf{Q}, \mathbf{P}) - D(\mathbf{Q}, \mathbf{P})) \boldsymbol{\beta} v \\ & \sim \partial_t \mathbf{a} v - \partial_{z_k} \left[\left(\partial_t (\mathbf{Q}_j + i\mathbf{P}_j) - s \hat{\sigma}_j + i s \partial_j B \right) Z_{jk}^{-1} \mathbf{a} v \right] + \frac{i}{2} s \partial_{z_k} Q_l \partial_{l_j} B Z_{jk}^{-1} \mathbf{a} v \\ & \quad - i \partial_{z_k} \left(\partial_j s Z_{jk}^{-1} (\hat{\sigma} \cdot \mathbf{P} + B) \mathbf{a} v \right) + \frac{i}{2} \partial_{z_k} Q_l \partial_{l_j} s Z_{jk}^{-1} (\hat{\sigma} \cdot \mathbf{P} + B) \mathbf{a} v \\ & \quad - s(\mathbf{Q}) \hat{\sigma} \cdot \mathbf{C}(\mathbf{Q}) \mathbf{a} v \end{aligned}$$

$$\begin{aligned} &\sim \partial_t \mathbf{a}v - \partial_{z_k} \left[(\partial_t(Q_j + iP_j) - s\hat{\sigma}_j + i\partial_j D(\mathbf{Q}, \mathbf{P})) Z_{jk}^{-1} \mathbf{a}v \right] \\ &\quad + \frac{i}{2} \partial_{z_k} Q_l \left[s\partial_{lj} B + \partial_{lj} s(\hat{\sigma} \cdot \mathbf{P} + B) \right] Z_{jk}^{-1} \mathbf{a}v - s(\mathbf{Q}) \hat{\sigma} \cdot \mathbf{C}(\mathbf{Q}) \mathbf{a}v. \end{aligned} \quad (2.24)$$

If we define

$$\mathbf{F}_j := (\partial_t(Q_j + iP_j) - s\hat{\sigma}_j + i\partial_j D) \mathbf{r} = \left(\partial_{P_j} h(\mathbf{Q}, \mathbf{P}) - s\hat{\sigma}_j - i\partial_{Q_j} h(\mathbf{Q}, \mathbf{P}) + i\partial_j D \right) \mathbf{r}, \quad (2.25)$$

then one can obtain $\mathbf{r}^\dagger \mathbf{F}_j = 0$ for $j=1,2$. Noticing that $\mathbf{a}(t, \mathbf{q}, \mathbf{p}) = a(t, \mathbf{q}, \mathbf{p}) \mathbf{r}(\mathbf{Q}, \mathbf{P})$ then (2.24) can be written as

$$\begin{aligned} i(h(\mathbf{Q}, \mathbf{P}) - D(\mathbf{Q}, \mathbf{P})) \beta v &\sim \partial_t \mathbf{a}v - \partial_{z_k} \left[a \mathbf{F}_j Z_{jk}^{-1} v \right] - s(\mathbf{Q}) \hat{\sigma} \cdot \mathbf{C}(\mathbf{Q}) \mathbf{a}v \\ &\quad + \frac{i}{2} \partial_{z_k} Q_l \left[s\partial_{lj} B + \partial_{lj} s(\hat{\sigma} \cdot \mathbf{P} + B) \right] Z_{jk}^{-1} \mathbf{a}v. \end{aligned} \quad (2.26)$$

Thus by solvability condition one gets

$$\mathbf{r}^\dagger \left\{ \partial_t \mathbf{a}v - \partial_{z_k} \left[a \mathbf{F}_j Z_{jk}^{-1} v \right] + \frac{i}{2} \partial_{z_k} Q_l \left[s\partial_{lj} B + \partial_{lj} s(\hat{\sigma} \cdot \mathbf{P} + B) \right] Z_{jk}^{-1} \mathbf{a}v - s(\mathbf{Q}) \hat{\sigma} \cdot \mathbf{C}(\mathbf{Q}) \mathbf{a}v \right\} = 0, \quad (2.27)$$

which implies an ODE for the scalar amplitude a

$$\begin{aligned} \frac{da}{dt} + \mathbf{r}^\dagger \left(\partial_{P_j} h \partial_{Q_j} \mathbf{r} - \partial_{Q_j} h \partial_{P_j} \mathbf{r} \right) a &= -\partial_{z_k} \mathbf{r}^\dagger \mathbf{F}_j Z_{jk}^{-1} - s(\mathbf{Q}) \mathbf{r}^\dagger \hat{\sigma} \cdot \mathbf{C}(\mathbf{Q}) a \\ &\quad - \frac{i}{2} \mathbf{r}^\dagger \partial_{z_k} Q_l \left[s\partial_{lj} B + \partial_{lj} s(\hat{\sigma} \cdot \mathbf{P} + B) \right] Z_{jk}^{-1} \mathbf{r} a. \end{aligned} \quad (2.28)$$

We notice that the field \mathbf{C} actually modifies the amplitude of the wave-packet, as it was already noticed for instance in [12, 30].

As a summary of this section, in the frozen Gaussian approximation, we compute

$$\psi_{\text{FGA},0} = \frac{1}{(2\pi\varepsilon)^3} \sum_{m=\pm} \int_{\mathbb{R}^6} \mathbf{a}_m(t, \mathbf{q}, \mathbf{p}) \exp\left(\frac{i}{\varepsilon} \Phi_m(t, \mathbf{y}, \mathbf{q}, \mathbf{p})\right) v_m(\mathbf{y}, \mathbf{q}, \mathbf{p}) d\mathbf{y} d\mathbf{q} d\mathbf{p}, \quad (2.29)$$

where \mathbf{a}_m , Φ_m , and v_m are defined in (2.10), (2.11), and (2.12), respectively, and \mathbf{Q}_m , \mathbf{P}_m , S_m , and a_m are determined by the evolutionary equations (2.13), (2.21), and (2.28). Finally, we have the following error estimate.

Theorem 2.1. For ρ smooth and bounded, and denoting ψ^ε be the solution of the Dirac equation and $\psi_{\text{FGA},0}$ be the corresponding FGA solution then for any $T > 0$, there exists a constant $C_T > 0$, such that for any $\varepsilon > 0$

$$\sup_{0 \leq t \leq T} \left\| \psi^\varepsilon - \psi_{\text{FGA},0} \right\|_{L^2} \leq \varepsilon C_T.$$

Proof. The proof is a straightforward extension of that in [7] for Dirac equation in flat space and in [20] for high frequency wave. \square

3 Numerical approximation

This section is devoted to the computation of FGA and numerical experiments. In particular, we will be interested in the comparison of the wave-packet propagation in curved spaces and in flat spaces, illustrating the focusing effect of graphene surfaces. We will also provide some qualitative comparisons between FGA and tight-binding solutions.

3.1 Numerical scheme

In this subsection, we give an overview of the algorithms involved in the computation of FGA.

- The Hamiltonian flow (2.13) is solved using a standard fourth-order Runge-Kutta method.
- Linear systems are solved using Gauss' elimination method (scaling and pivoting).
- Fourier and Inverse Fourier transforms are performed using FFT.
- The FBI and inverse FBI transforms are performed as in [8].
- Transparent boundary conditions are trivial within the framework of FGA. Indeed, whenever a Gaussian profile $Q(t)$ no longer belongs to the computational domain Ω its contribution is removed from the FGA.
- Let us notice that the parallelization of the FGA computation can be trivially performed by following the procedure in [18] for the non-relativistic regime.

More technical details of the above algorithms can be found in [8].

3.2 Numerical experiments

In this section, we propose to numerically illustrate the FGA on given graphene surfaces \mathcal{S} . In particular, we will compare the wave-function evolution on flat and strained graphene surfaces. The Dirac equation under consideration is constructed from a diagonal metric expressed in isothermal coordinates $ds^2 = v_F dt^2 - \rho(\mathbf{r}) d\mathbf{r}$. As recalled in the introduction, the transformation from Cartesian (where the metric tensors are usually not diagonal for non-flat surfaces) to isothermal coordinates requires the solution to a Beltrami equation and allows to calculate ρ from the parameterization of the surface in Cartesian coordinates. In this paper, we then assume that the function ρ is given, and we describe the evolution of the wave-function directly in isothermal coordinates. The deformation of the graphene surfaces induces a pseudo-magnetic field \mathbf{A} , which is defined in (1.9), and a spin affine connection denoted by \mathbf{C} . The latter is however perturbative

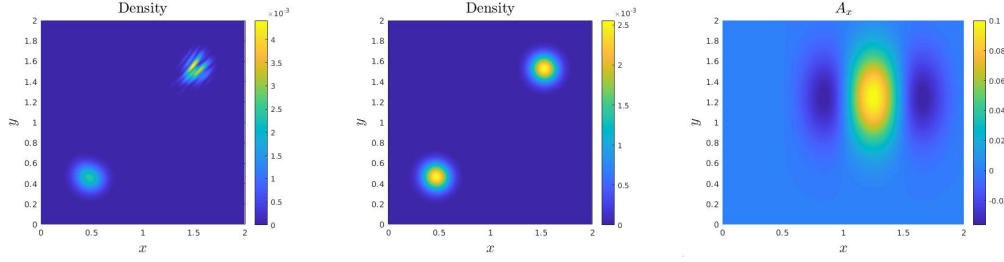


Figure 1: **Experiment 1.** Density at $T=0.5$ for strained (left) and flat (middle) graphene surfaces. (Right) Graph of A_x .

($C = \mathcal{O}(\varepsilon)$), and we hence neglect this contribution in the simulations. The numerical experiments are performed on eight GPU processors and take approximately 5 seconds for $\varepsilon = 2^{-8}$. As explained above, a standard PDE solver would require much more CPU time. We first propose to illustrate the convergence of the FGA as a function of ε .

Experiment 1. This first experiment is devoted to the propagation of a wave-packet on a strained graphene surface, in the semi-classical regime. Rather than defining the graphene surface in Cartesian coordinates, then constructing the corresponding Dirac equation in isothermal coordinates (which would require long and tedious calculations and the solution to a Beltrami equation, see [14]), we propose to directly start from the Dirac equation written in isothermal coordinates. The Dirac equation is then solved in this system of coordinates using the FGA derived above. In this experiment, we also compare the propagation of this wave-packet on a flat surface. We assume below that $\varepsilon = 10^{-8}$, the computational domain is $\Omega = (0, 2)$ and with $\Delta t = 5 \times 10^{-3}$; we consider 150 times iterations and the maximum number of Gaussian beams is fixed to 4×10^7 . The initial wave-function is given by (3.1)

$$\omega_I(\mathbf{x}) = (\exp(-a|\mathbf{x} - \mathbf{x}_0|^2), 0)^T, \quad (3.1)$$

with $a=20$, $\mathbf{x}_0=(1,1)$, $S_I(\mathbf{x})=\mathbf{p}_0 \cdot \mathbf{x}$, and $\mathbf{p}_0=(1,1)$. We compare the propagation of a wave-packet on a flat graphene surface and strained one. The latter one is defined thanks to its metric and more specifically the function ρ in the metric (1.2) and A_x (A_y is taken null) is given by

$$\rho(\mathbf{x}) = 1 + b_1 \exp(-300|\mathbf{x} - \mathbf{x}_1|^2), \quad A_x(\mathbf{x}) = b_2 \cos(2\pi(x-1)) \exp(-5|\mathbf{x} - \mathbf{x}_1|^2), \quad (3.2)$$

with $b_1 = 2.5 \times 10^{-1}$, $b_2 = 10^{-1}$ and $\mathbf{x}_1 = (1.25, 1.25)$. Notice that $b_1 = b_2 = 0$ corresponds to the flat case. We report the density at final time in Fig. 1 (left). We also report the corresponding solution in flat space (middle). We also report the graph of A_x in Fig. 1 (right).

Experiment 2. In order to validate the derived computational model, we propose to *qualitatively* compare the evolution of the solution to the FGA with the solution to a time-dependent tight-binding model. The latter is a standard approach for modeling pristine

and strained graphene surfaces [24]. Let us indeed recall that from the following time-dependent Schrödinger equation,

$$i\partial\psi = \mathcal{H}\psi, \quad \text{with} \quad \mathcal{H} = -\Delta + V(x,y),$$

where V is a periodic potential on an infinite hexagonal lattice, where each lattice point represents the position of a Carbon atom. From this model, one can derive the so-called “tight-binding” operator which reads, using the second-quantization, as follows:

$$\mathcal{H}_{TB} = -\sum_{\mathbf{r}'} t_{\mathbf{r}',\delta'(\mathbf{r})} c_{\mathbf{r}'}^\dagger c_{\mathbf{r}'+\delta'(\mathbf{r})} + \text{Hermitian Conjugate},$$

where $c_{\mathbf{r}'}$ (resp. $c_{\mathbf{r}'}^\dagger$) represents the creation (resp. annihilation) operator and where \mathbf{r}' (resp. \mathbf{r}) represented the position of Carbon atoms on the strained (resp. pristine) lattice, and $\mathbf{r}'+\delta'(\mathbf{r})$ the positions of the nearest neighbor. We typically consider

$$t_{\mathbf{r}',\delta'(\mathbf{r})} = t_0 \exp(-\beta|\delta'(\mathbf{r})|/a-1),$$

where t_0 (resp. a) is the hopping parameter (resp. inter-atomic distance) on the pristine graphene surface, and β is the Grüneisen parameter [17]. The function $t_{\mathbf{r}',\delta'(\mathbf{r})}$ models the overlap between the orbitals for nearest Carbon atoms, which is then space-dependent due to the surface deformation. The Dirac equation introduced in our paper is actually derived from the tight-binding model in the low energy limit or equivalently in the vicinity of the Dirac point [24]. The objective here is not a quantitative comparison (which will be proposed in a forthcoming paper), but rather to show that at least qualitatively, the FGA solution allows to describe the dynamics of electron on a deformed graphene surface at a much cheaper cost. We refer to [6,24] for details. In the following, we consider a Gaussian graphene surface with the same structure as the one used in the above example. The computations for the tight-binding model are performed using `kwant` [15] and `pybinding` [23] libraries. We report the density of electron from Dirac/FGA and from tight-binding model with the same Gaussian deformation but with 2 distinct standard deviations (Gaussian “width”). What is proposed below, rather than an accurate comparison between the tight-binding and Dirac solutions (which would require a very fine and more advanced analysis), is the effect of the broadening of the Gaussian deformation. For the FGA case, we assume that $\varepsilon = 10^{-8}$, and the computational domain is $\Omega = (0,2)$, $\Delta t = 5 \times 10^{-4}$, we consider 150 times iterations and the maximum number of Gaussian beams is fixed to 4×10^7 . The initial wave-function is given by (3.1) and

$$\rho(\mathbf{x}) = 1 + b_1 \exp(-b_2|\mathbf{x} - \mathbf{x}_1|^2), \quad (3.3)$$

with $b_1 = 2.5 \times 10^{-1}$, $b_2 = 30$ (resp. 300) in (3.3) and $\mathbf{x}_1 = (1.25, 1.25)$. We observe that i) the wavefunction is focused thanks to the deformation, and that ii) when the deviation of the Gaussian deformation is reduced the wavefunction is split in mainly 2 parts, see Fig. 2. Similarly, we propose a comparison of the tight-binding solutions when the standard deviation of the Gaussian deformation is changed. As in the FGA case, we observe

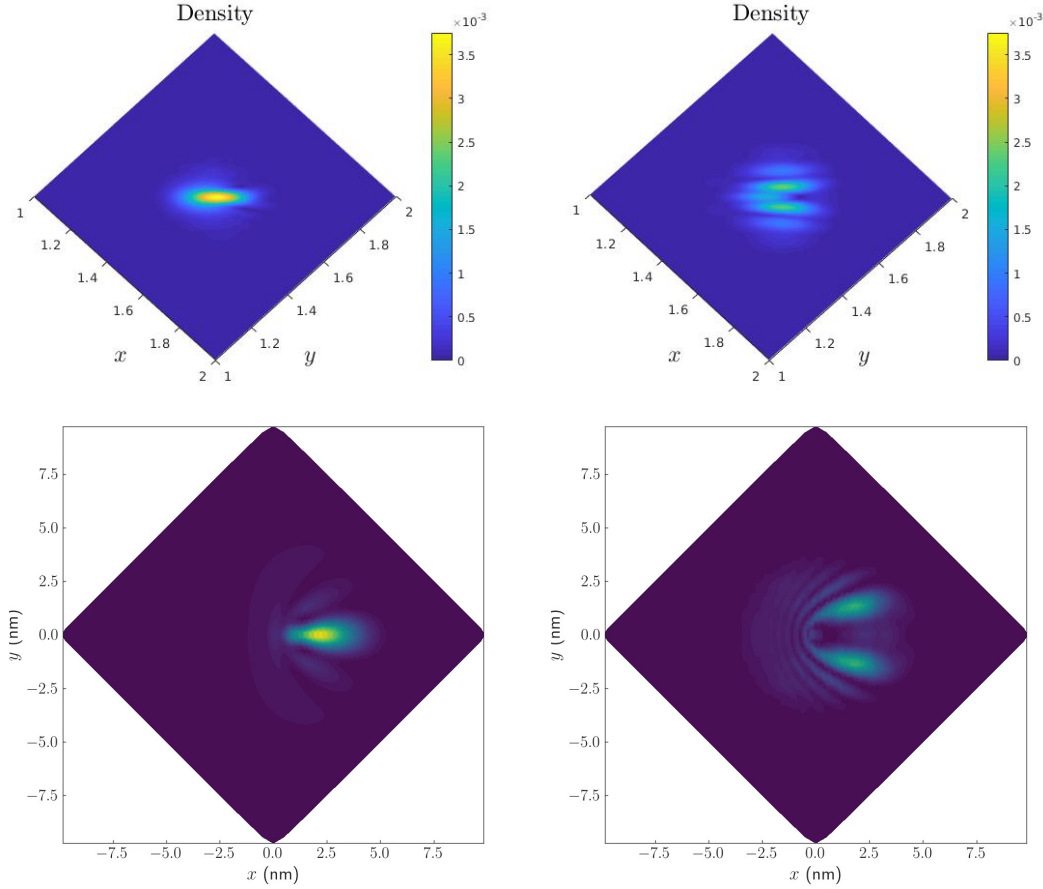


Figure 2: **Experiment 2.** (Top-left) FGA solution at $T=0.75$ with $b_2=30$. (Top-right) FGA solution at $T=0.75$ with $b_2=300$ (Bottom-Left) Tight-binding with standard deviation 2.5. (Bottom-right) Tight-binding with standard deviation 0.25.

i) the focusing of the wavefunction, and ii) its splitting in mainly 2 parts when the standard deviation of the Gaussian deformation is reduced by a factor of 10 (2.5 and 0.25). This comparison, although only qualitative, allows to justify the relevance and further investigation of the studied Dirac model and its approximation by FGA.

Experiment 3. We consider the same data as **Experiment 1.** but with a magnitude $b = 1$ in (3.2), $a = 40$ in (3.1) and no external field. The density is reported in Fig. 3, on a flat graphene surface (left) and on deformed graphene surface (right). In Fig. 4, we compare four classical electron trajectories on strained ($b = 1$) and flat surfaces ($b = 0$) in order to illustrate the focusing effect of deformation.

For the sake of completeness of the study, we also compare the electron trajectories computed with Evans' model [13]. In this goal, we represent the trajectories of electrons classically modeled by (1.13). We consider 4 distinct initial states $\mathbf{Q}_0 = (1, 0.88)$,

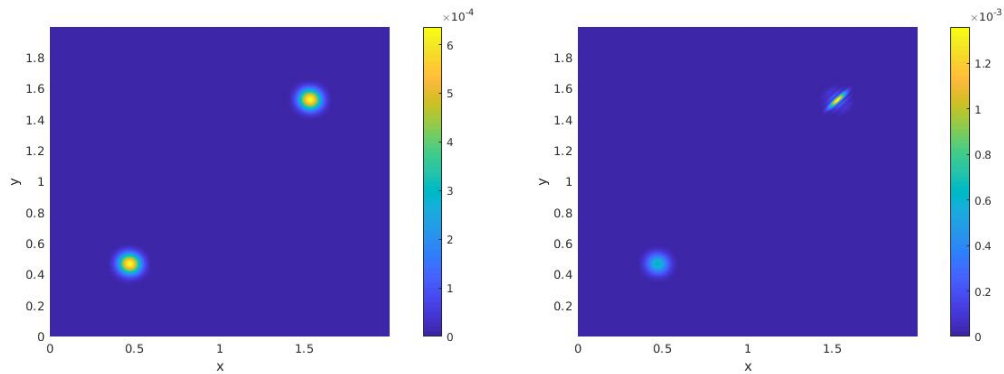


Figure 3: **Experiment 3.** Density at final time $T=0.75$. (Left) Flat space. (Right) Curved space. By comparing the shape of upright corner wave-packets, one can see the focusing effect caused by strained graphene.

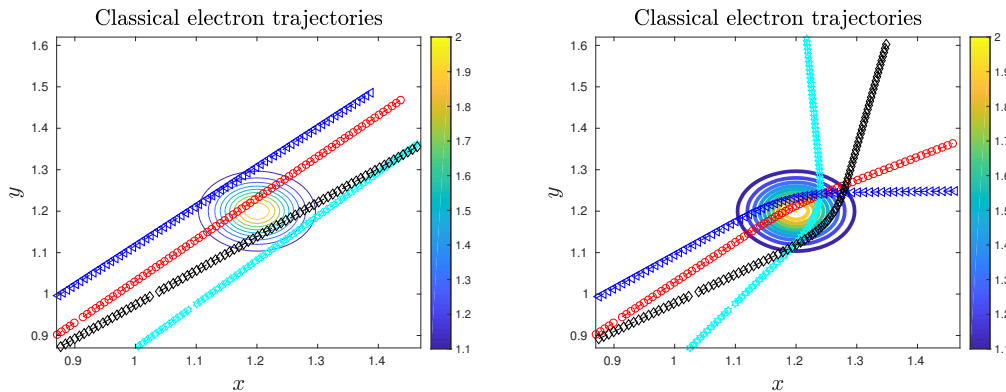


Figure 4: **Experiment 3.** We present four classical electron trajectories $\{Q(t), t \in [0, 0.75]\}$ on flat (left) and strained (right) surfaces for $b=0$ and $b=1$ in (3.2), respectively. Here we plot the circles as the level sets of the function ρ with $b=1$ to indicate the location of strain and show the focusing effect of deformation.

$(0.93, 1.05)$, $(0.97, 0.95)$, $(0.96, 0.98)$, n_0 close to 0.9, and $\rho(x) = 1 + \exp(-|x - x_0|^2)$ with $x_0 = (1.2, 1.2)$. A second order ODE solver is used to compute the electron-rays in the vicinity of the deformed surface. This is reported in Fig. 5. The corresponding trajectories are relatively close to the one computed with FGA.

Experiment 4. In this last experiment, we propose a comparison of the CPU-time between the FGA and the IMEX pseudospectral method developed in [2,3] for solving the Dirac equation. The spatial and time domains, time step, and strained graphene surfaces are fixed. In the case of the pseudospectral (resp. FGA) method, the number of grid points in real space (resp. the total number of Gaussians) is multiplied by 2 in each direction, when ϵ is divided by 2. As it is observed in Fig. 6, when ϵ is small, the FGA is more efficient than a pseudospectral approximation of the Dirac equation.

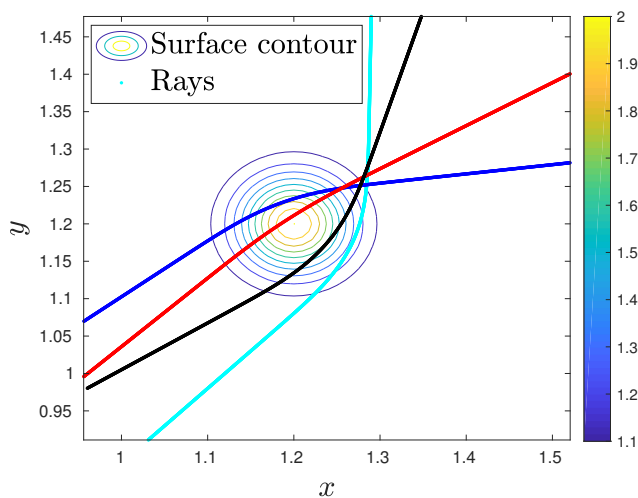


Figure 5: **Experiment 3.** Classical electron trajectories from Evans' model.

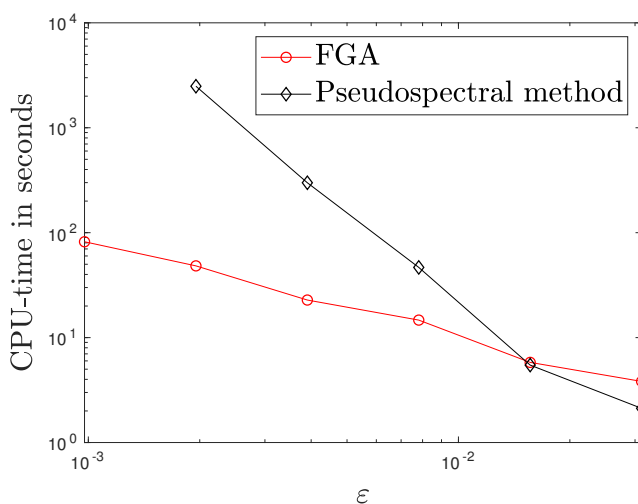


Figure 6: **Experiment 4.** CPU-time in logscale as a function of ε (CPU-time scaling) for FGA and IMEX pseudospectral methods.

4 Conclusion

In this paper, we proposed the frozen Gaussian approximation (FGA) for computing the solution to the Dirac equation in curved space in the semi-classical regime. The focusing and split effects of wavefunctions due to the deformation of graphene surfaces were illustrated by numerical comparisons of the Dirac solutions on curved and flat spaces. We

also present The CPU-time comparison shows that FGA becomes more efficient than the IMEX pseudospectral method when ε is small. In addition, the trajectories of electrons computed by FGA agree well with those from Evans' model.

Acknowledgments

L.C. was partially supported by the NSFC Projects Nos. 12271537 and 11901601. E.L. was partially supported by NSERC through the Discovery Grant program. X.Y. was partially supported by the NSF grants DMS-1818592 and DMS-2109116.

Appendix: Eigenvalues and eigenvectors

In order to derive the amplitude equation, we need to explicitly construct ∂h and ∂r . First notice

$$\begin{aligned}\partial_Q h_{\pm} &= \mp s(Q) \frac{(P_l - A_l) \partial_Q A_l}{|P - A(Q)|} + \partial_Q s(Q) |P - A(Q)|, \\ \partial_P h_{\pm} &= \pm s(Q) \frac{(P - A)}{|P - A(Q)|}, \\ \partial_{P_j} \partial_{Q_k} h_{\pm} &= \pm s(Q) \frac{(P_j - A_j)(P - A) \cdot \partial_{Q_k} A}{|P - A(Q)|^3} \mp s(Q) \frac{\partial_{Q_k} A_j}{|P - A(Q)|} \pm \partial_{Q_j} s(Q) \frac{(P_k - A_k)}{|P - A(Q)|}, \\ \partial_{P_j} \partial_{P_k} h_{\pm} &= \mp s(Q) \frac{(P_j - A_j)(P_k - A_k)}{|P - A(Q)|^3} \pm s(Q) \frac{\delta_{jk}}{|P - A(Q)|}, \\ \partial_{Q_j} \partial_{Q_k} h_{\pm} &= \mp s(Q) \frac{(P - A) \cdot \partial_{Q_j} A (P - A) \cdot \partial_{Q_k} A}{|P - A(Q)|^3} \pm s(Q) \frac{\partial_{Q_j} A \cdot \partial_{Q_k} A - (P - A) \cdot \partial_{Q_j} \partial_{Q_k} A}{|P - A(Q)|} \\ &\quad \mp \partial_Q s(Q) \frac{(P_l - A_l) \partial_Q A_l}{|P - A(Q)|} + \partial_{Q_j} \partial_{Q_k} s(Q) |P - A(Q)|.\end{aligned}$$

We recall that the classical trajectories are modeled by

$$\frac{d^2 Q}{dt^2} = -\partial_{PP} h(Q, P) \partial_Q h(Q, P) + \partial_{QP} h(Q, P) \partial_P h(Q, P), \quad Q(0, q, p) = q, \quad P(0, q, p) = p.$$

Hence

$$\partial_z r = \partial_z Q_j \partial_{Q_j} r + \partial_z P_j \partial_{P_j} r. \quad (\text{A.1})$$

References

- [1] L. V. Ahlfors. *Lectures on Quasiconformal Mappings*, volume 38. American Mathematical Soc., 2006.

- [2] X. Antoine, F. Fillion-Gourdeau, E. Lorin, and S. MacLean. Pseudospectral computational methods for the time-dependent Dirac equation in static curved spaces. *J. Comput. Phys.*, 411:109412, 24, 2020.
- [3] X. Antoine and E. Lorin. Computational performance of simple and efficient sequential and parallel Dirac equation solvers. *Comput. Phys. Commun.*, 220:150–172, 2017.
- [4] P. Bracken. Metric geometry and the determination of the bohmian quantum potential. *Journal of Physics Communications*, 3(6), 2019.
- [5] A. H. Castro Neto, F. Guinea, N. M. R. Peres, K. S. Novoselov, and A. K. Geim. The electronic properties of graphene. *Rev. Mod. Phys.*, 81:109–162, Jan 2009.
- [6] A.H. Castro Neto, F. Guinea, N.M.R. Peres, K.S. Novoselov, and A.K. Geim. The electronic properties of graphene. *Reviews of Modern Physics*, 81(1):109–162, 2009.
- [7] L. Chai, J. Hateley, E. Lorin, and X. Yang. On the convergence of frozen gaussian approximation for linear non-strictly hyperbolic systems. *Commun. Math. Sci.*, 19(3), 2021.
- [8] L. Chai, E. Lorin, and X. Yang. Frozen gaussian approximation for the Dirac equation in semi-classical regime. *SIAM J. Num. Anal.*, 57:2383–2412, 2019.
- [9] A. J. Chaves, T. Frederico, O. Oliveira, W. de Paula, and M. C. Santos. Optical conductivity of curved graphene. *Journal of Physics: Condensed Matter*, 26(18):185301, Apr 2014.
- [10] S-S. Chern. An elementary proof of the existence of isothermal parameters on a surface. *Proceedings of the American Mathematical Society*, 6(5):771–782, 1955.
- [11] C. Colijn and E.R. Vrscaj. Spin-dependent bohm trajectories for pauli and dirac eigenstates of hydrogen. *Foundations of Physics Letters*, 16(4):303–323, 2003.
- [12] F. de Juan, J. L. Mañes, and M. A. H. Vozmediano. Gauge fields from strain in graphene. *Phys. Rev. B*, 87:165131, Apr 2013.
- [13] J. Evans and M. Rosenquist. " $F = ma$ " optics. *American Journal of Physics*, 54(10):876–883, 1986.
- [14] F. Fillion-Gourdeau, E. Lorin, and S. Maclean. Numerical quasiconformal transformations for electron dynamics on strained graphene surfaces. *Physical Review E*, 103(1), 2021.
- [15] C. W. Groth, M. Wimmer, A. R. Akhmerov, and X. Waintal. Kwant: A software package for quantum transport. *New Journal of Physics*, 16, 2014.
- [16] M.F. Herman and E. Kluk. A semiclassical justification for the use of non-spreading wavepackets in dynamics calculations. *Chemical Physics*, 91(1):27–34, 1984.
- [17] M.I. Katsnelson. *Graphene: Carbon in Two Dimensions*, volume 9780521195409. 2012.
- [18] E. Lorin, X. Yang, and X. Antoine. Frozen Gaussian approximation based domain decomposition methods for the linear Schrödinger equation beyond the semi-classical regime. *J. Comput. Phys.*, 315:221–237, 2016.
- [19] J. Lu and X. Yang. Frozen Gaussian approximation for high frequency wave propagation. *Commun. Math. Sci.*, 9(3):663–683, 2011.
- [20] J. Lu and X. Yang. Convergence of frozen Gaussian approximation for high-frequency wave propagation. *Comm. Pure Appl. Math.*, 65(6):759–789, 2012.
- [21] J. Lu and X. Yang. Frozen Gaussian approximation for general linear strictly hyperbolic systems: formulation and Eulerian methods. *Multiscale Model. Simul.*, 10(2):451–472, 2012.
- [22] G. M. Maksimova, V. Ya. Demikhovskii, and E. V. Frolova. Wave packet dynamics in a monolayer graphene. *Phys. Rev. B*, 78:235321, Dec 2008.
- [23] D. Moldovan, M. Andelkovic, and F. Peeters. pybinding v0.9.5: A python package for tight-binding calculations (v0.9.5). <https://doi.org/10.5281/zenodo.4010216>, 2020.
- [24] G. G. Naumis, S. Barraza-Lopez, M. Oliva-Leyva, and H. Terrones. Electronic and optical properties of strained graphene and other strained 2D materials: A review. *Reports on*

- Progress in Physics*, 80(9), 2017.
- [25] Z. Hua Ni, T. Yu, Y.H. Lu, Y. Y. Wang, Y. P. Feng, and Z. X. Shen. Uniaxial strain on graphene: Raman spectroscopy study and band-gap opening. *ACS Nano*, 2(11):2301–2305, 2008. PMID: 19206396.
 - [26] M.D. Pollock. On the dirac equation in curved space-time. *Acta Physica Polonica B*, 41(8), 2010.
 - [27] T. Swart and V. Rouse. A mathematical justification for the Herman-Kluk propagator. *Comm. Math. Phys.*, 286(2):725–750, 2009.
 - [28] B. Thaller. *The Dirac Equation*. Texts and Monographs in Physics. Springer-Verlag, Berlin, 1992.
 - [29] A. L. Valerian. Conformality with respect to Riemannian metrics. *Annales academi scientiarum fennicae series A. I. Mathematica*, 206:1–22, 1955.
 - [30] G.E. Volovik and M.A. Zubkov. Emergent Horava gravity in graphene. *Annals of Physics*, 340(1):352–368, Jan 2014.
 - [31] H. Wu, Z. Huang, S. Jin, and D. Yin. Gaussian beam methods for the Dirac equation in the semi-classical regime. *Communications in Mathematical Sciences*, 10(4):1301–1315, 2012.
 - [32] X. Yang and J. Zhang. Computation of the Schrödinger equation in the semiclassical regime on an unbounded domain. *SIAM J. Numer. Anal.*, 52(2):808–831, 2014.